

# Development and analysis of 3D ionosphere modeling using base functions and GPS data over Iran

Mir-Reza Ghaffari Razin<sup>1</sup>

Received: 13 September 2014/Accepted: 12 April 2015/Published online: 29 April 2015  
© Akadémiai Kiadó 2015

**Abstract** In this study, a 3D-model of the electron density has been performed using the global positioning system (GPS) measurements over Iran. 2D spherical harmonic functions and empirical orthogonal functions are used as base functions to model the horizontal and the vertical content of the electron density, respectively. The ionosonde data in Tehran ( $\varphi = 35.7382^\circ$ ,  $\lambda = 51.3851^\circ$ ) has been used for choosing an optimum value for the regularization parameter. To apply the method for constructing a 3D-image of the electron density, GPS measurements of the Iranian permanent GPS network (at 3-day in 2007) have been used. The instability of solution has been numerically analyzed and the Tikhonov method has been used for regularizing the solution. To come up with an optimum regularization parameter, the relative error in electron density profile computed from ionosonde measurements and their 3D model are minimized. The modeling region is between  $24^\circ$  to  $40^\circ\text{N}$  and  $44^\circ$  to  $64^\circ\text{W}$ . The result of 3D-Model has been compared to that of the international reference ionosphere model 2012 (IRI-2012). The data analysis shows that the latitudinal section of ionosphere electron density from 3D technique supports the expected time and height variations in ionosphere electron density. Moreover, these findings show that the height of maximum electron density is changed during the day and night and confirms the efficiency of multi-layer models in comparison to single-layer models. This method could recover 64–99 % of the ionosphere electron density.

**Keywords** Ionosphere modeling · Total electron contents · Ionosonde · Regularization · GPS · IRI 2012

---

✉ Mir-Reza Ghaffari Razin  
rghaffari@mail.kntu.ac.ir

<sup>1</sup> Department of Geodesy and Geomatics Engineering, K. N. Toosi University of Technology, No. 1346, Vali\_Asr Ave., Mirdamad Cr., Tehran, Iran

## 1 Introduction

During the last decades, GPS has become a common tool for analyzing the earth's atmosphere. Ionospheric refraction is one of the main error sources on GPS signals. This effect is proportional to the total electron content (TEC). The International GNSS Service (IGS) uses its dense global GNSS ground stations to compute global ionospheric TEC maps on a routine basis (Hernández-Pajares et al. 2009). With the development of regional and local permanent GPS networks such as the SOPAC in Europe, the spatial and temporal resolution of such studies has been considerably increased as compared to the traditional meteorological techniques.

In the customary two dimensional modeling techniques, ionosphere is approximated by a thin spherical shell of free electrons, located; 250–450 km from the surface of the earth. The existing two dimensional methods of modeling the electron density can be classified to non-grid based and grid based techniques (El-Arini et al. 1995). The former modeling techniques are based on the least squares estimation of a functional model for certain types of observables derived from the GPS carrier phase and code measurements. Polynomials and spherical harmonics are some of the base functions that are commonly in use (Walker 1989; Komjathy 1997; Schaer 1999; Coster et al. 2003). In grid based modeling, the spherical shell of free electrons is developed into a grid of rectangular elements, then special reconstruction algorithms are used for estimating the electron density within the every element of the shell (El-Arini et al. 1993, 1994; Gao et al. 1994; Skone 1998; Liao 2000; Liao and Gao 2001). Neglecting the vertical gradient of the electron density is the main deficiency of the two dimensional modeling techniques. Specially, during high solar activity; this gradient and its impact on TEC is large (Komjathy 1997). Moreover, analyzing such variations to any accuracy is not possible due to dimensionality restriction of the model. These limitations led to the development of the multi-layer and tomography models.

The application of the tomographic reconstruction to three dimensional modeling of the electron density using radio waves was proposed in (Austen et al. 1988) and applied by Andreeva et al. (1990). These results encouraged the further analysis and development of this method (Raymund et al. 1993; Foster et al. 1994; Mitchell et al. 1997; Yin et al. 2004; Yizengaw et al. 2007; Strangeways et al. 2009; Amerian et al. 2010). Generally, the tomographic models can be categorized as function based models and voxel based models. In the former approach, the electron density ( $N_e$ ) is developed into a set of analytical base functions which account for the horizontal and vertical variations of  $N_e$  within the ionosphere (Howe et al. 1998; Hansen et al. 1997; Liao and Gao 2001). The system of simultaneous equations to be solved for estimating  $N_e$  in this approach is ill conditioned. Therefore, the application of regularization techniques for obtaining a reliable solution is needed. In the voxel based method; the ionosphere is developed into a set of cubic elements whose electron density is estimated using special reconstruction algorithms (Raymund et al. 1993; Hansen et al. 1997; Hernández-Pajares et al. 1999; Colombo et al. 1999). The rank deficiency of the system of simultaneous equations to be solved for estimating  $N_e$  in every cubic element is an inherent property of the voxel based approach. In this paper, the function based tomographic reconstruction is used for analyzing the three-dimensional structure of the electron density in Iran. Direct estimates of the electron density obtained from the ionosonde station are used for this purpose.

The paper is organized as follows: in Sect. 2, the methodology for extraction of ionospheric information from GPS observations is presented. The function based slant total

electron content (STEC) modeling using harmonics and empirical orthogonal functions is studied in Sects. 3 and 4. In Sect. 5, an appropriate procedure for the estimation of the unknown series coefficients is introduced. Finally, in Sect. 6, the procedure is applied to real GPS data, which were collected from observation sites in Iran.

## 2 Input parameters

Dual frequency GPS receivers provide carrier phase  $\Phi_i$  ( $i = 1, 2$ ) and code  $P_i$  ( $i = 1, 2$ ) observations on L-band ( $L_1, L_2$ ) frequencies (Seeber 1993):

$$P_1 = \rho + c(dt - dT) + c(\tau_{P1}^S + \tau_{P1}^r) + I_1 + d_{trop} + \varepsilon_{P1}, \quad (1)$$

$$P_2 = \rho + c(dt - dT) + c(\tau_{P2}^S + \tau_{P2}^r) + I_2 + d_{trop} + \varepsilon_{P2}, \quad (2)$$

$$\Phi_1 = \rho + c(dt - dT) + c(T_{L1}^S + T_{L1}^r) + \lambda_1 N_1 - I_1 + d_{trop} + \varepsilon_{L1}, \quad (3)$$

$$\Phi_2 = \rho + c(dt - dT) + c(T_{L2}^S + T_{L2}^r) + \lambda_2 N_2 - I_2 + d_{trop} + \varepsilon_{L2}, \quad (4)$$

$$I_i = \frac{40.3}{f_i^2} STEC, \quad (5)$$

where  $P_1, P_2, \Phi_1$  and  $\Phi_2$  are the code and carrier phase pseudo-ranges on the  $L_1$  and  $L_2$  signals, respectively;  $\rho$  is the geometric range between receiver and satellite (m),  $c$  is the speed of light (m/s),  $dt$  is the satellite clock error with respect to GPS time (s),  $dT$  is the receiver clock error with respect to GPS time (s), frequency dependent terms  $\tau^S, \tau^r, T^S$  and  $T^r$  which are due to the satellite and receiver hardware delays are known as code and phase inter-frequency biases (IFBs),  $\lambda_i$  is the wavelength of the GPS signal on  $L_i$  frequency,  $N_i$  is the carrier phase integer ambiguity (cycle),  $d_{trop}$  is the troposphere delay (m),  $I_i$  is the ionospheric delay (m) and  $\varepsilon$  is the measurement noise (m). In order to benefit from the ambiguity independent estimates of STECs derived from the code pseudo-ranges as well as the high precision of carrier phase measurements, code pseudo-ranges are smoothed using “carrier to code leveling process” (Ciraolo et al. 2007; Nohutcu et al. 2010). Using code and carrier phase observations in both frequencies, we can compute ionospheric observable as follow (Ciraolo et al. 2007):

$$STEC = (\tilde{P}_4 - br - bs - \langle \varepsilon_P \rangle_{arc} + \varepsilon_L) \frac{f_1^2 f_2^2}{40.3(f_2^2 - f_1^2)} \quad (6)$$

In Eq. (6) STEC is the input observation for tomography method in TECU (1TECU =  $1 \times 10^{16}$  el./m<sup>2</sup>),  $\tilde{P}_4$  is the pseudo range ionospheric observable smoothed with the carrier-phase ionospheric observable,  $br = c(\tau_{P1}^r - \tau_{P2}^r)$  and  $bs = c(\tau_{P1}^S - \tau_{P2}^S)$  are the code differential inter-frequency biases for the receiver and satellite, respectively and  $f_1$  and  $f_2$  are GPS signal frequency.

### 3 Development of a 3D model

The total electron content (TEC) represents the total number of electrons in a column along the direction of a satellite (sv) to a receiver (rx) (Coster et al. 2003). It can be expressed as:

$$\begin{aligned} STEC &= \int_{rx}^{sv} N_e(\lambda, \varphi, h) ds = \int_{rx}^{sv} [N_0(\lambda, \varphi, h) + \delta N_e(\lambda, \varphi, h)] ds \\ &= \int_{rx}^{sv} N_0(\lambda, \varphi, h) ds + \int_{rx}^{sv} \delta N_e(\lambda, \varphi, h) ds \end{aligned} \quad (7)$$

In which, STEC is the input observation obtained from Eq. (6),  $N_e(\lambda, \varphi, h)$  denotes the ionospheric electron density function at the position  $(\lambda, \varphi, h)$ . The ionospheric electron density function  $N_e(\lambda, \varphi, h)$  can be written as the sum of two parts  $N_0(\lambda, \varphi, h)$  and  $\delta N_e(\lambda, \varphi, h)$ . The approximate value of the deterministic portion  $N_0(\lambda, \varphi, h)$  can be obtained from historical ionospheric electron density data or from the output of empirical ionosphere models and  $\delta N_e(\lambda, \varphi, h)$  is the corresponding correcting term which is sought in order to improve the accuracy of the empirical estimate  $N_0(\lambda, \varphi, h)$ . The integral of the deterministic part of electron density function along the GPS signal path from satellite to receiver is defined as  $STEC_0$ :

$$STEC_0 = \int_{rx}^{sv} N_0(\lambda, \varphi, h) ds \quad (8)$$

In function based approach to reconstruct the electron density, the correction term  $\delta N_e(\lambda, \varphi, h)$  is developed into a set of horizontal and vertical base functions. Spherical harmonic functions (SHFs) and empirical orthogonal functions (EOFs) are normally used as the horizontal and the vertical base functions respectively. The degree and order of the spherical harmonic functions depends on the acquired spatial resolution and the required accuracy (Liu and Gao 2001a, b; Liu 2004):

$$\delta N(\lambda, \varphi, h) = \sum_{k=1}^K \sum_{m=-M}^M \sum_{n=|m|}^M [a_{nk}^m \cos(m\lambda) + b_{nk}^m \sin(m\lambda)] \bar{P}_n^m(\cos \varphi) Z_k(h), \quad (9)$$

where  $\bar{P}_n^m(\cos \varphi)$  is the normalized Legendre function of degree  $m$  and order  $n$ ,  $Z_k(h)$  is the empirical orthogonal function,  $a_{nk}^m$ ,  $b_{nk}^m$  are the model coefficients to be determined by solving the simultaneous system of Eq. (7),  $K$  denotes the highest order of empirical orthogonal functions and  $M$  denotes the highest order of spherical harmonics functions. The rest task of ionospheric tomography is to optimally estimate the model coefficients in Eq. (9) in which the number of the unknown model parameters is determined by the truncation limits of SHFs and EOFs.

In the data analysis presented in Sect. 6 the highest order of SHFs is chosen to 4 ( $M = 4$ ). After extensive calculation and parameterization comparisons, it is found that using the order of SHFs as 4 could produce highest modeling accuracies. For the vertical component the highest order of EOFs is 3 ( $K = 3$ ). The number of actually estimated ionospheric coefficients is equal to  $K(M + 1)(2M + 1)$ , consequently in this paper 135 ionospheric parameters used for modeling. Combining Eqs. (6), (7), (8) and (9) results in the fundamental observation equation in the function based 3D reconstruction of the electron density as:

$$\begin{aligned}
& (\tilde{P}_4 - br - bs - \langle \varepsilon_P \rangle_{arc} + \varepsilon_L) \frac{f_1^2 f_2^2}{40.3(f_2^2 - f_1^2)} - STEC_0 \\
& = \sum_{k=1}^K \sum_{m=-M}^M \sum_{n=|m|}^M a_{nk}^m \int_{rx}^{sv} \cos(m\lambda) \bar{P}_n^m(\cos \varphi) Z_k(h) ds \\
& + \sum_{k=1}^K \sum_{m=-M}^M \sum_{n=|m|}^M b_{nk}^m \int_{rx}^{sv} \sin(m\lambda) \bar{P}_n^m(\cos \varphi) Z_k(h) ds
\end{aligned} \tag{10}$$

#### 4 Empirical orthogonal functions (EOFs)

EOFs are derived from empirical data of the ionospheric electron density, which can be obtained from an empirical ionospheric model such as the International Reference Ionosphere (IRI) model or the direct measurements which are related to the electron density (such as ionosonde measurements) (Bilitza and Reinisch 2008). IRI model provides an initial estimate for the vertical profile of the electron density at any desired location in space and time. Having the samples of the density profile obtained at different times and heights, the matrix of electron density profile could be formed as:

$$N(t, h) = \begin{bmatrix} N(t_1, h_1) & N(t_1, h_2) & \dots & N(t_1, h_N) \\ N(t_2, h_1) & N(t_2, h_2) & \dots & N(t_2, h_N) \\ \dots & \dots & \dots & \dots \\ N(t_M, h_1) & N(t_M, h_2) & \dots & N(t_M, h_N) \end{bmatrix} \tag{11}$$

in which,  $N(t_i, h_j)$  is electron density in height  $h_j$  ( $j = 1, 2, \dots, N$ ) and epoch  $t_i$  ( $i = 1, 2, \dots, M$ ). The mean value of each column ( $\bar{N}(h_j)$ ) in this matrix provides an estimate for the mean value of the electron density at a given height:

$$\bar{N}(h_j) = \frac{1}{M} \sum_{m=1}^M N(t_m, h_j) \tag{12}$$

The vertical variation of the electron density within the area of study (at an arbitrary epoch  $t$ ) can be analyzed using the variation matrix  $S$  below:

$$S = \tilde{N}^T(t, h) \tilde{N}(t, h) \tag{13}$$

In which,  $\tilde{N}(t, h)$  is a matrix containing per column the difference between the corresponding elements of matrix  $N$  from the mean value  $\bar{N}(h_j)$  (Bjornsson and Venegas 1997). In mathematical statistics, the method of principal component analysis is used to explore the vertical variations that are inherent in Eq. (13) (Jackson 2003). For this purpose, the principal (also known as empirical orthogonal) components of matrix  $S$  are firstly computed. Then, the contribution of every component to the total variations is analyzed.

**Theorem 1** If  $x = [x_1, \dots, x_p]^T$  is a vector of random variables whose variance covariance matrix is  $\Sigma$ , the linear combinations  $y_h = e_h^T x$  in which  $e_h$  is the  $h$ th eigenvector of  $\Sigma$  is known as a principal component of this matrix. The corresponding eigenvalue  $\lambda_h$  is the variance of this principal component (Johnson and Wichern 2002). Since the trace of the

**Table 1** The eigenvalue of S matrix and its corresponding principal component

Eigenvalue	EOF (%)
1.49E+09	88.60
1.98E+08	11.39
343,910.8	0.021
117.42	0.000007

variance covariance matrix of a random variable is equal to the sum of its eigenvalue, the ratio of every eigenvalue ( $\lambda_i$ ) to this sum ( $\sum \lambda_i$ ) is a measure for the contribution of the corresponding principal component to the total variation expressed by this summation. To come up with an optimum number of empirical orthogonal functions to account for the vertical variations of the electron density in the adopted 3D reconstruction technique, the contribution of the empirical orthogonal functions of matrix  $S$  (Eq. 13) have been computed and compared using the equation  $\lambda_i \times 100 / \sum \lambda_i$ . Table 1 demonstrates these results.

The empirical orthogonal functions whose contribution in the total variation expressed by the sum of the eigenvalue of  $S$  are less than 98 % of the total variation have been ignored. To create matrices  $S$  and  $N$ , IRI-2012 model (Bilitza and Reinisch 2008) is employed. According to the obtained results, the first three eigenvalues of matrix  $S$  include 98 % of the total variations of the electron density. Therefore, the first three EOFs have been used for modeling the vertical variations of the electron density in this research. The first three vertical basis functions from IRI-2012 model are given in Fig. 1.

In this paper, analytical forms of the three EOFs are considered (in writing these functions, MATLAB curve fitting toolbox is used):

$$\begin{aligned} Z_1(h) &= \alpha_1 h^3 + \alpha_2 h^2 + \alpha_3 h + \alpha_4 \\ Z_2(h) &= \alpha_1 h^4 + \alpha_2 h^3 + \alpha_3 h^2 + \alpha_4 h + \alpha_5 \\ Z_3(h) &= \alpha_1 h^4 + \alpha_2 h^3 + \alpha_3 h^2 + \alpha_4 h + \alpha_5 \end{aligned} \quad (14)$$

In Eq. (14),  $\alpha_1, \alpha_2, \alpha_3, \alpha_4$  and  $\alpha_5$  are EOFs coefficients.

## 5 Parameter estimation

In matrix notation, the observations Eq. (10) may be re-written in the following form:

$$\mathbf{d} = \mathbf{Gm} + \mathbf{v} \quad (15)$$

In which  $\mathbf{d}$  is the observation vector whose elements are the values of  $\delta\text{STEC} = \text{STEC} - \text{STEC}_0$ ,  $\mathbf{m}$  is the vector of unknown parameters, i.e. the coefficients  $a_{nk}^m$  and  $b_{nk}^m$ ,  $\mathbf{G}$  is the design or the coefficient matrix of the model and  $\mathbf{v}$  is the observation noise vector. In Eq. (15) design matrix has the following form:

$$\mathbf{G} = \left[ \begin{array}{ccccccccc} h_{11} & h_{12} & \dots & h_{1n} & F & 0 & \dots & 0 & F & 0 & \dots & 0 \\ h_{21} & h_{22} & \dots & h_{2n} & 0 & F & \dots & 0 & 0 & F & \dots & 0 \\ \dots & \dots \\ h_{m1} & h_{m2} & \dots & h_{mn} & 0 & 0 & \dots & F & 0 & 0 & \dots & F \end{array} \right] \quad (16)$$

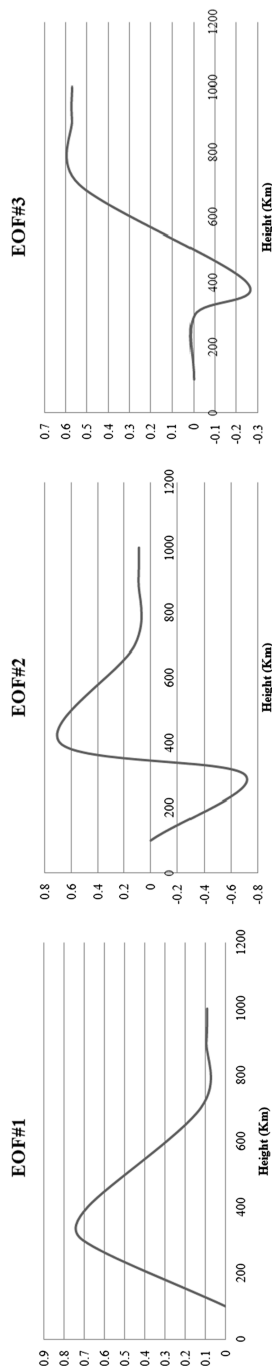


**Fig. 1** Vertical basis functions from IRI-2012 model

In this matrix  $F$  defined as follows:

$$F = \frac{f_1^2}{40.3(1 - \gamma)} \quad (17)$$

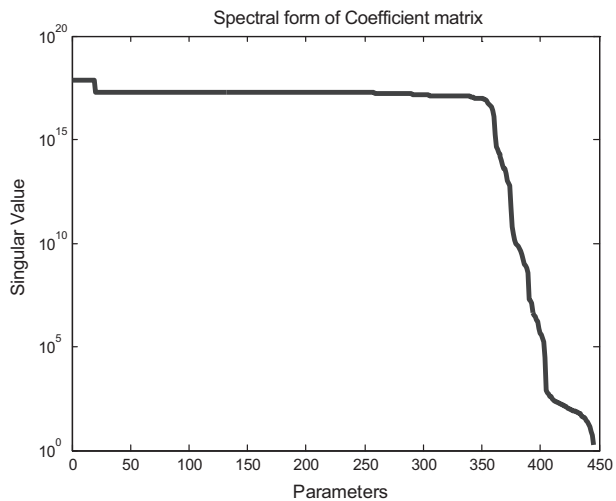
In design matrix  $\mathbf{G}$ , the first sub-matrix shows the spherical harmonic coefficients, second sub-matrix indicates receiver inter frequency bias and third sub-matrix shows satellite inter frequency bias. Also in design matrix  $\mathbf{h}$  defined as follows:

$$\begin{aligned} h_{i,j} &= \int_{rx}^{sv} \cos(m\lambda) \bar{P}_n^m(\cos \phi) Z_k(h) ds \\ h_{i,l} &= \int_{rx}^{sv} \sin(m\lambda) \bar{P}_n^m(\cos \phi) Z_k(h) ds \end{aligned} \quad (18)$$

The integral Eq. (10) is a Fredholm integral equation of the first kind. It is mathematically proved that such integral equations are improperly posed in the sense that the solution of their corresponding system of simultaneous equations is not a continuous function of the input parameters (Hansen 1987). The spectral decomposition of the coefficient matrix can provide an immediate insight into the instability of solution for a system of simultaneous equations. The spectral form of the design matrix is shown in Fig. 2. In this figure horizontal axis illustrates the unknown parameters and vertical axis indicates singular values of coefficient matrix.

The asymptotic decay of the spectral values is an indication for the discontinuity of the solution because, for such a system of simultaneous equations, the condition number is large and thereby perturbations of the input parameters are magnified on the outputs. The following equation provides an upper bound limit for the perturbations of the model parameters  $\mathbf{m}$  as a function of the perturbations of input vector  $\mathbf{d}$  (Jain et al. 2003):

**Fig. 2** Spectral form of coefficient matrix



$$\frac{\|\tilde{\mathbf{m}} - \mathbf{m}\|}{\|\mathbf{m}\|} \leq k(\mathbf{G}) \frac{\|\tilde{\mathbf{d}} - \mathbf{d}\|}{\|\mathbf{d}\|}, \quad k(\mathbf{G}) = \frac{\sigma_{\max}}{\sigma_{\min}}, \quad (19)$$

where  $\tilde{\mathbf{m}}$  and  $\tilde{\mathbf{d}}$  are the perturbed model parameters and input vector respectively and  $k(\mathbf{G})$  is the condition number of the matrix  $\mathbf{G}$  and  $\sigma_{\max}$  and  $\sigma_{\min}$  are the largest and smallest singular values of  $\mathbf{G}$ . To analyze the conditioning of the problem in further detail, the discrete Picard condition can be used (Hansen 1987). The corresponding discrete Picard condition is illustrated in Fig. 3. This figure indicates the problem is ill-conditioned.

Although the Picard condition provides an upper bound limit for the regularization error of a regularized solution, it can also be used for analyzing the instability of the least-squares solution to Eq. (15) (Mashhadi Hossainali 2006): The Picard condition is a necessary condition for a stable least-squares solution. To come up with a stable solution for the model parameters, the application of regularization techniques is inevitable. In this paper, Tikhonov–Philips first order regularization technique (Hansen 1987; Aster et al. 2003) has been used for this purpose. In this method, regularized solution satisfies the following criterion:

$$\min \| \mathbf{G}\mathbf{m} - \mathbf{d} \|_2^2 + \alpha^2 \| \mathbf{m} \|_2^2 \quad (20)$$

In which  $\alpha$  is known as regularization parameter and controls the instability and resolution of solution. Regularized solution is computed using:

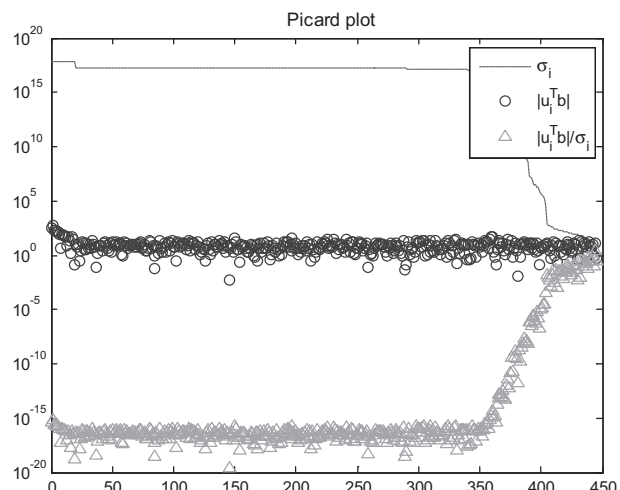
$$\mathbf{m}_x = (\mathbf{G}^T \mathbf{G} + \alpha^2 \mathbf{L})^{-1} \mathbf{G}^T \mathbf{d} \quad (21)$$

In Eq. (21)  $\mathbf{L}$  is a positive definite matrix which takes different forms according to the order of regularization. For zeroth-order Tikhonov regularization  $\mathbf{L} = \mathbf{I}$  (identity matrix).

## 6 Numerical results

Iran geodynamic studies started since 1998 to monitor the variations in the earth's crust and tectonic movements. Permanent GPS network was designed and implemented gradually in 2004 to investigate the mechanisms of active faults in Iran. This network

**Fig. 3** Discrete Picard condition



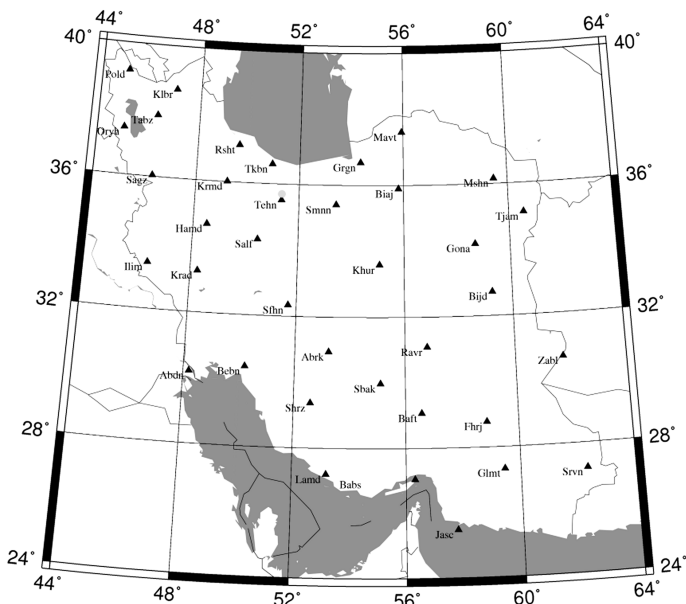


**Fig. 4** The spatial distribution of the GPS and ionosonde station (green circle) of this study. (Color figure online)

currently has 120 permanent GPS stations in the initial phase. Average distance between dense parts is about 25–30 km. From these 120 stations, 40 stations are selected for modeling ionospheric electron content over Iran in January 3, 2007, April 3, 2007 and July 13, 2007. Figure 4 illustrates the spatial distribution of the stations as well as the ionosonde station ( $\phi = 35.7382^\circ$ ,  $\lambda = 51.3851^\circ$ ) available in this region. Ionosonde provides direct measurements of the ionospheric electron density. The sampling rate of the measurements is 30 s and the adopted elevation cut-off angle for the observations is  $15^\circ$ . In this paper, 2-hour intervals are used to process GPS observations and ionosphere behaviors.

To analyze the efficiency of the reconstructed 3D-model in estimating the electron density outside of the study area, electron density has been computed and compared to the electron density obtained from the direct measurements at the ionosonde station and IRI2012 model. Since the outputs of the ionosonde station of Tehran are given at just one height for each epoch, a height profile of the electron density cannot be derived. Therefore, a point-wise comparison of the modeled electron density and the ionosonde results is inevitable. Tables 2, 3 and 4 give the relative error of the computed electron density in different time and heights. The relative errors demonstrate the error percentage in the electron density prediction using tomography method and IRI2012 electron density with respect to the ionosonde results.

In these tables it is seen that, for each time epoch in which the relative error of IRI prediction is high; the relative error of reconstructed electron density reduces significantly and the predicted electron density closely approximates the ionosonde measurements. Small values of relative errors for estimated electron densities support the accurate estimation of this parameter using the proposed method. Also in these tables, minimum relative error between reconstructed electron density and ionosonde measurements is

**Table 2** Reconstructed electron density and electron density from the ionosonde measurement on January 03, 2007 (in  $10^{11}$  ele/m $^3$ )

Time (UT)	Altitude (km)	Reconstructed electron density	Ionosonde measurements	IRI 2012 electron density	Relative error (%) GPS-RE and ionosonde	Relative error (%) IRI 2012 and ionosonde
1	278	1.1017	0.9842	0.9554	-11.9173	-2.93
3	233	0.6535	0.8382	1.0192	+5.8667	21.59
5	223	3.1521	3.7104	3.0561	+15.0468	-17.63
7	227	8.74	10.7716	4.1553	+18.8607	-61.42
9	219	3.9388	4.100	4.2434	+3.9305	3.50
11	226	4.9308	5.1910	3.7681	+5.0136	-27.41
13	211	3.1642	3.1375	2.2095	-0.8530	-29.58
15	198	2.9245	2.5111	0.5659	-16.4629	-77.46
17	244	1.3895	1.1310	0.6488	-22.8558	-42.63
19	247	1.0756	1.1917	0.3141	+9.7427	-73.64
21	319	1.1865	1.3751	1.1660	+13.7153	-15.21
23	281	0.7724	0.9378	1.4976	+17.6370	59.69

**Table 3** Reconstructed electron density and electron density from the ionosonde measurement on April 03, 2007 (in  $10^{11}$  ele/m $^3$ )

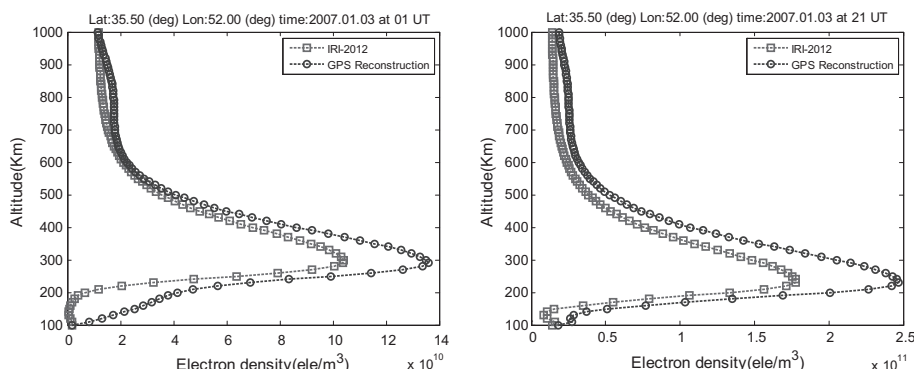
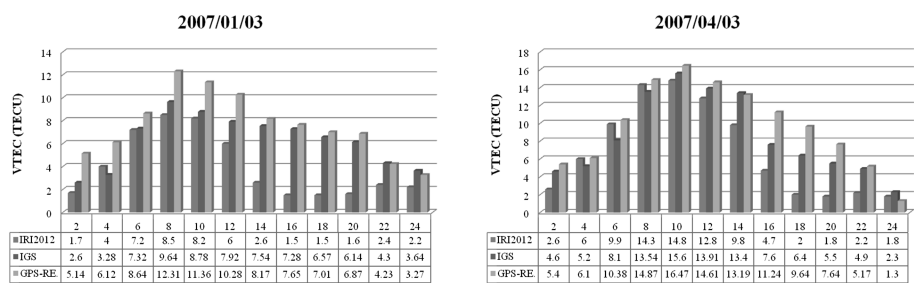
Time (UT)	Altitude (km)	Reconstructed electron density	Ionosonde measurements	IRI 2012 electron density	Relative error (%) GPS-RE and ionosonde	Relative error (%) IRI 2012 and ionosonde
1	251	0.5934	0.7262	0.7077	+18.280	-2.550
3	222	2.1658	2.9049	2.0528	+25.443	-29.33
5	253	3.9699	4.6598	3.6371	+14.805	-21.95
7	302	7.2134	7.8376	5.2142	+7.9641	-33.47
9	257	9.1519	9.6468	7.1975	+5.1301	-25.39
11	232	5.5804	5.7848	6.2770	+3.5338	8.510
13	236	5.2575	4.3901	6.0118	-17.756	36.94
15	217	4.0839	3.5229	2.9923	-15.924	-15.06
17	275	1.5218	1.6702	1.6394	+8.8851	-1.840
19	292	1.2489	1.3260	0.7807	+5.8144	-41.12
21	268	1.6920	1.6071	0.6174	-5.2828	-61.58
23	244	1.3154	1.2937	0.3118	-1.6773	-75.90

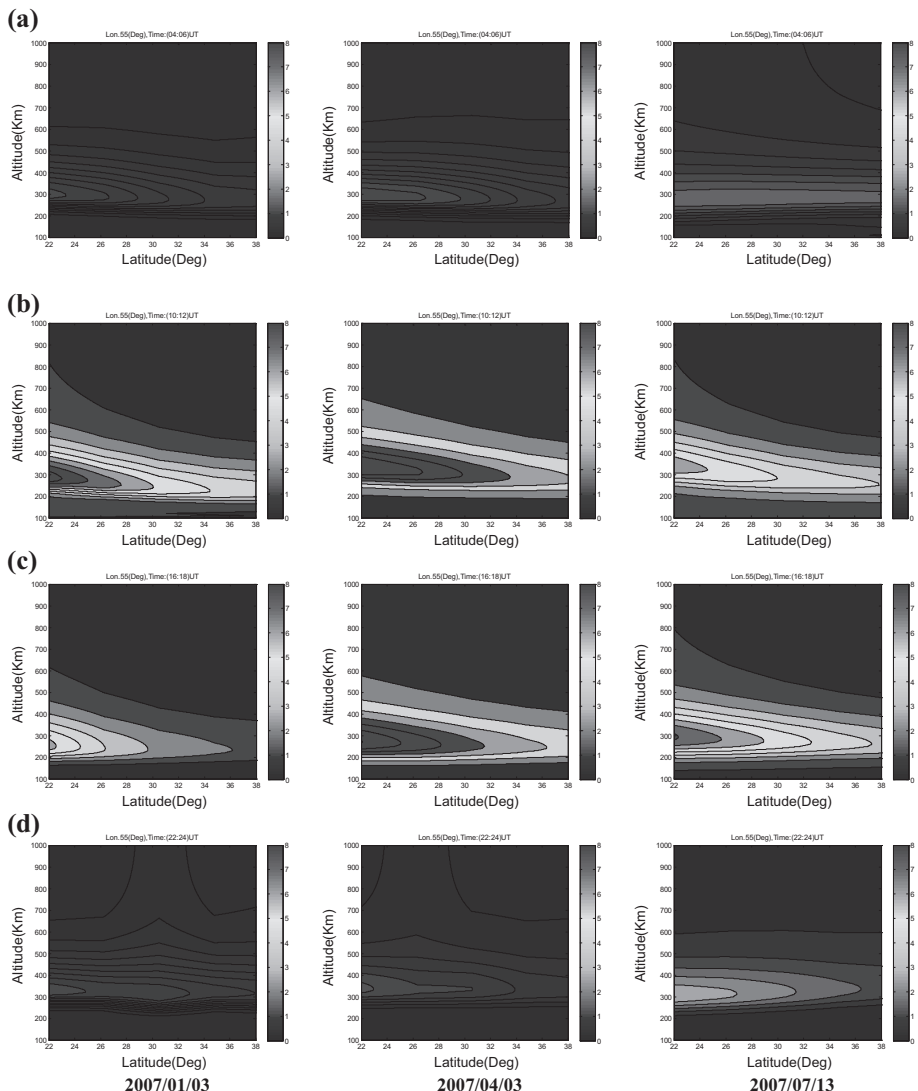
0.85 % and maximum relative error is 36.44 %. These results indicate that the reconstructed 3D-model is able to recover 64–99 % of the ionosphere electron density.

Figure 5 demonstrate the comparison between reconstructed electron density profile and electron density profile from International Reference Ionosphere model 2012 (IRI 2012) at 01 UT and 21 UT. In this figure, squares are the IRI extracted data in 10 km intervals. Illustrated circles at this figure give the three-dimensional estimate of electron density.

**Table 4** Reconstructed electron density and electron density from the ionosonde measurement on July 13, 2007 (in  $10^{11}$  ele/m $^3$ )

Time (UT)	Altitude (km)	Reconstructed electron density	Ionosonde measurements	IRI 2012 electron density	Relative error (%) GPS-RE and ionosonde	Relative error (%) IRI 2012 and ionosonde
1	245	0.9740	1.2461	0.8157	+21.8361	-34.54
3	217	2.6589	2.7979	2.1465	+4.9680	-23.28
5	292	4.2193	4.1716	2.7978	-1.1434	-32.93
7	269	4.8465	4.5090	3.6823	-7.4850	-18.33
9	319	3.4150	3.7104	3.6832	+7.9614	-0.73
11	335	4.0254	3.8889	3.0207	-3.5099	-22.33
13	251	3.9865	4.2875	3.8920	+7.0204	-9.22
15	277	2.9654	2.7393	4.1779	-8.2539	52.52
17	245	3.9879	3.5893	1.8244	-11.105	-49.17
19	236	3.9235	3.2254	0.7057	-21.6431	-78.12
21	219	1.2485	1.9643	0.2208	+36.440	-88.76
23	271	1.8763	1.5191	0.8668	-20.5139	-42.94

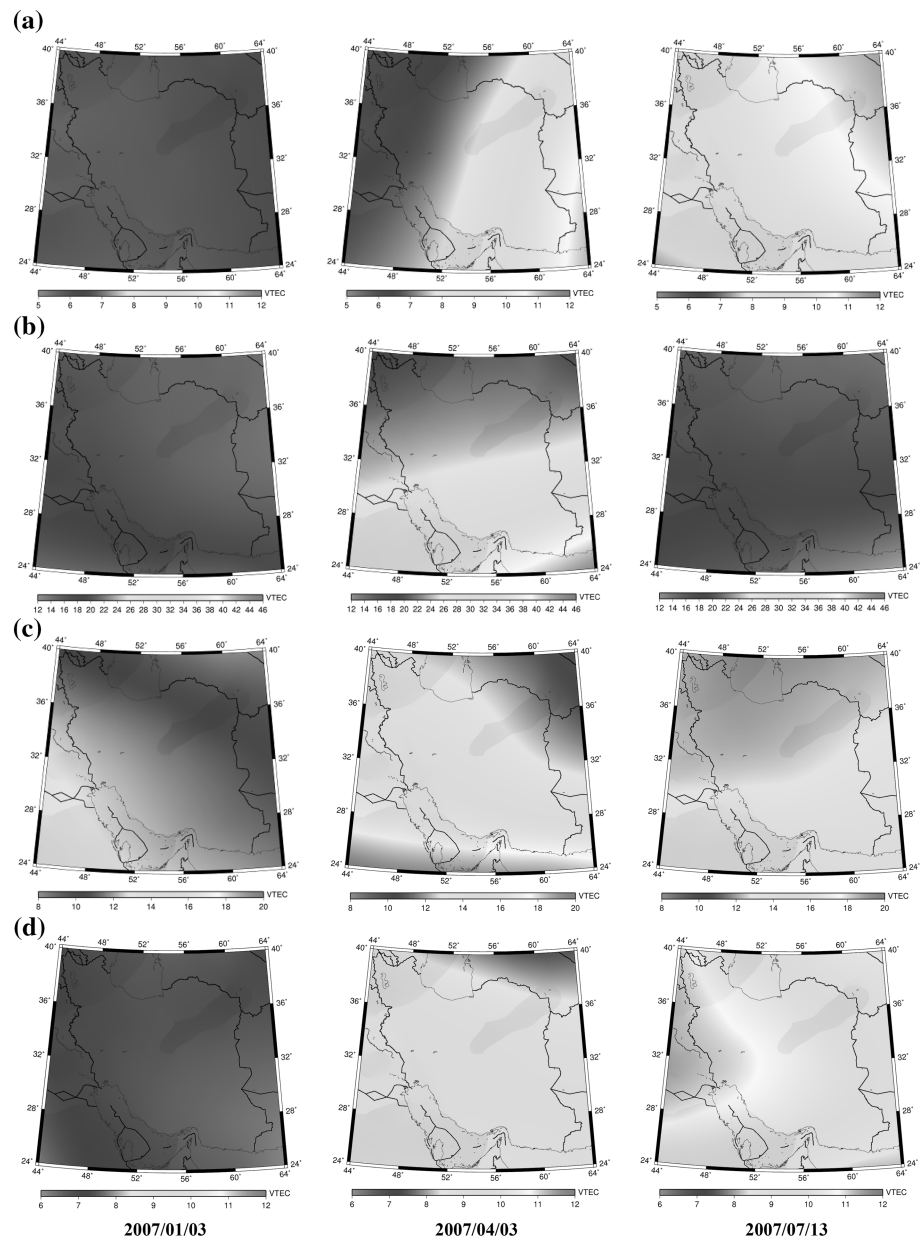
**Fig. 5** Comparison between reconstructed electron density profile and IRI 2012 profile**Fig. 6** Comparison of reconstructed VTEC, IRI2012 VTEC and IGS VTEC in TECU ( $10^{16}$  ele/m $^2$ ), left related to 2007/01/03 and right related to 2007/04/03



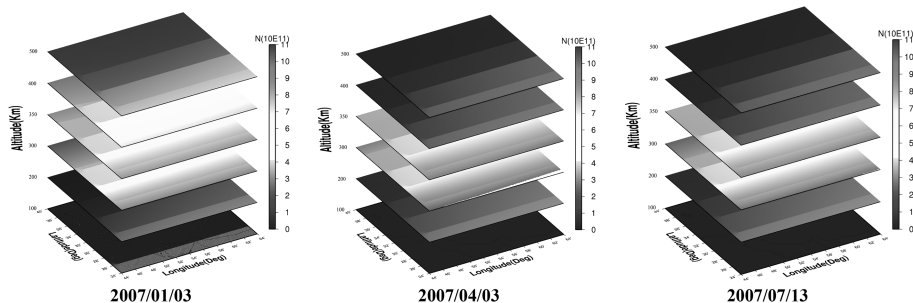
**Fig. 7** Latitudinal profiles of electron density ( $10^{11}$  ele/m $^3$ ) on 3 days of 2007 at 4 time intervals, two times in day-side and two times in night-side. **a** Latitudinal profiles of electron density ( $10^{11}$  ele/m $^3$ ) in 3 days of 2007 at 04–06 UT **b** latitudinal profiles of electron density ( $10^{11}$  ele/m $^3$ ) in 3 days of 2007 at 10–12 UT **c** latitudinal profiles of electron density ( $10^{11}$  ele/m $^3$ ) in 3 days of 2007 at 16–18 UT **d** latitudinal profiles of electron density ( $10^{11}$  ele/m $^3$ ) in 3 days of 2007 at 22–24 UT

Figure 6 shows that the different reconstructed TEC values derived from 3D method and IRI 2012 model as well as IGS product during all 12 time intervals in 2007/01/03 and 2007/04/03. The results of this comparison confirm the validity of proposed method in ionosphere reconstruction.

To analyze the vertical variations of the electron density developed by the reconstructed model, vertical profiles of the reconstructed image have been obtained every 2 h and these are drawn at a fixed longitude of 55°E. These profiles are shown in Fig. 7. It is seen that the



**Fig. 8** The model estimates of VTEC at four times in 3 days of 2007, the *left panel* indicate results of 2007/01/03, *middle panel* 2007/04/03 and *right panel* 2007/07/13. **a** map of VTEC horizontal variations in 3-days of 2007 at 02 UT **b** map of VTEC horizontal variations in 3-days of 2007 at 08 UT **c** map of VTEC horizontal variations in 3-days of 2007 at 14 UT **d** map of VTEC horizontal variations in 3-days of 2007 at 20 UT



**Fig. 9** The model estimates of electron density at six height layer in 3 days of 2007, the *left panel* indicate results of 2007/01/03, *middle panel* 2007/04/03 and *right panel* 2007/07/13

electron density reaches its maximum value between 10 and 12 universal time (UT). The height of maximum electron density is between 250 and 350 km above the surface of the earth. Moreover, daily variation in the height of maximum electron density is remarkable in these results; on the other hand, the peak of the electron density value between the day-side and the night-side is different. This corresponds to the expected diurnal variations of electron density. These characteristics which are the constituents of the ionosphere morphology in three dimensions are also reported elsewhere (Liu and Gao 2001a, b; Yizengaw et al. 2007) and confirmed by the analysis of the direct measurement techniques.

Figure 8 illustrates the horizontal variations of VTEC over study area (Iran) at 3 days of 2007 suggested by the developed 3D method (in  $10^{16} \text{ m}^2$ ). After estimation of electron density in desired geographical locations for 10 km height interval using 3D model, Eq. (7) is used to compute TEC values. All figures drawn at four time interval: two times in day-side and two times in night-side. The main purpose of drawing these maps is indicating the horizontal variations in ionosphere electron content. In other words, the 3D model developed in this paper is able to reconstruct horizontal variations of TEC.

Also using developed model, we are able to estimate the ionosphere electron density at different height layers. Figure 9 indicates results of 3D model at six height layers in 3 days of 2007. All figures have been drawn at 02 UT.

According to the results in Fig. 9, ionosphere electron density variations are the highest value in the range of 300–400 km. Unlike 2D ionosphere models that a fixed height are considered for ionospheric variations, 3D model is able to indicate electron density variations in each desire height layer.

## 7 Conclusions

In this study, the function-based tomography technique has been used for reconstructing a 3D model of the electron density using the GPS measurements of the Iranian permanent GPS network. In this method, spherical harmonics and empirical orthogonal functions are the base functions in use for modeling the horizontal and the vertical variations of the electron density. In comparison with the voxel based model, the function based method explained in this paper, requires smaller number of parameters to characterize the ionosphere. The analysis for GPS network presented in this paper, shows that using 135 ( $M = 4, K = 3$ ) ionospheric parameters can demonstrate the ionosphere layer. If we use

the voxel based method for same network, we require 400–1200 parameters for represents the ionosphere. The reduced number of parameters will be significantly beneficial for real time applications. The variable to be modeled in the function based method is the electron density. The electron density is a fundamental parameter for describing the ionosphere. The function based model also has benefit of modeling the ionosphere in multiple layers. The data analysis shows that the latitudinal sections of the electron density in ionosphere obtained from the 3D technique support the expected time and height variations in the electron density. Moreover, these findings show that the height of maximum electron density is changed during the day and night. This confirms the efficiency of the developed multi-layer model in comparison to the traditional single-layer ones.

## References

- Amerian Y, Mashhadi Hossainali M, Voosoghi B, Ghaffari MR (2010) Tomographic reconstruction of the ionospheric electron density in term of wavelets. *J Aerosp Sci Technol* 7(1):19–29
- Andreeva ES, Galinov AV, Kunitsyn VE, Mel'nicenko YA, Tereshchenko ED, Filimonov MA, Chernykov SM (1990) Radiotomographic reconstructions of ionization dip in the plasma near the Earth. *J Exp Theor Phys Lett* 52:145–148
- Aster RC, Borchers B, Thurber C (2003) Parameter estimation and inverse problems. Elsevier Academic Press, New York
- Austen JR, Franke SJ, Liu CH (1988) Ionospheric imaging using computerized tomography. *Radio Sci* 23(3):299–307
- Bilitza D, Reinisch BW (2008) International reference ionosphere 2007: improvements and new parameters. *Adv Space Res* 42(4):599–609. doi:10.1016/j.asr.2007.07.048
- Bjornsson H, Venegas SA (1997) A manual for EOF and SVD analyses of climate data. Department of Atmospheric and Oceanic Sciences and Center for Climate and Global Change Research, McGill University, February, 1997, 53
- Ciraolo L, Azpilicueta F, Brunini C, Meza A, Radicella SM (2007) Calibration errors on experimental slant total electron content (TEC) determined with GPS. *J Geod* 81(2):111–120. doi:10.1007/s00190-006-0093-1
- Colombo O.L, Hernandez-Pajares M, Juan J.M, Snaz J, Talaya J (1999), Resolving carrier-phase ambiguities on the fly, at more than 100 km from nearest reference site, with the help of ionospheric tomography. In: Proceeding of ION GPS-99, Nashville, Sep 1999, pp. 1635–1642
- Coster AJ, Foster J, Erickson P (2003) Monitoring the Ionosphere with GPS. *Space Weather GPS World* 14(5):42–49
- El-Arini MB, O'Donnell PA, Kellam P, Klobuchar JA, Wisser TC, Doherty PH (1993) The FAA wide area differential GPS (WADGPS) static ionosphere experiment. In: Proceeding of the institute of navigation NTM-93, San Francisco, CA, Jan 1993
- El-Arini MB, Hegarty CJ, Fernow JP, Klobuchar JA (1994) Development of an error budget for a GPS wide-area augmentation system (WAAS). In: Proceeding of the institute of navigation NTM-94, San Diego, CA, Jan 1994
- El-Arini MB, Conker RS, Albertson TW, Reagan JK, Klobuchar JA, Doherty PH (1995) Comparison of real-time ionosphere algorithms for a gps wide-area augmentation system (WAAS). *J Inst Navig* 41(4):393–413 winter 1994–1995
- Foster JC, Buonsanto MJ, Klobuchar JA, Holt JM, Fougere P, Pakula WA, Raymund TD, Kunitsyn VE, Andreeva ES, Tereschenko ED, Kudukon BZ (1994) Russian American tomography experiment. *Int J Imag Syst Technol* 5:148–159
- Gao Y, Heroux P, Kouba J (1994) Estimation of GPS receiver and satellite L1/L2 signal delay biases using data from CACS. In: Processing of KIS-94, Banff, Aug 30–Sep 2 1994
- Hansen PC (1987) The truncated SVD as a method for regularization. *BIT* 27:534–553
- Hansen AJ, Walter T, Enge P (1997), Ionospheric correction using tomography. In: Proceeding of 10th international technical meeting of the satellite division of the institute of navigation, ION GPS-97, Sep 16–19
- Hernández-Pajares M, Juan JM, Sanz J (1999) New approaches in global ionospheric determination using ground GPS data. *J Atmos Sol Terr Phys* 61(16):1237–1247. doi:10.1016/S1364-6826(99)00054-1

- Hernández-Pajares M, Juan JM, Sanz J, Orus R, García-Rigo A, Feltens J, Komjathy A, Schaer SC, Krankowski A (2009) The IGS VTEC maps: a reliable source of ionospheric information since 1998. *J Geod* 83(3–4):263–275. doi:10.1007/s00190-008-0266-1
- Howe BM, Runsiman K, Secan JA (1998) Tomography of ionosphere: four dimensional simulations. *Radio Sci* 33(1):109–128
- Jackson JE (2003) A users' guide to principal components. Wiley, Hoboken
- Jain MK, Iyengar SRK, Jain RK (2003) Numerical methods for scientific and engineering computation. New Age International (P) Limited, Publishers, New Delhi
- Johnson RA, Wichern DW (2002) Applied multivariate statistical analysis. Prentice Hall, Upper Saddle River
- Komjathy A (1997) Global ionospheric total electron content mapping using the global positioning system. PhD dissertation, Department of Geodesy and Geomatics Engineering, Technical Report No. 188, University of New Brunswick, p 248
- Liao X (2000) Carrier phase based ionosphere recovery over a regional are GPS network. UCGE reports, number 20143, The University of Calgary, Calgary
- Liao X, Gao Y (2001) High-precision ionosphere TEC recovery using a regional-area GPS network. *Navigation* 48(2):101–111
- Liu ZZ (2004) Ionosphere tomographic modeling and applications using global positioning system (GPS) measurements. UCGE reports, number 20198, University of CALGARY, Jun 2004
- Liu ZZ, Gao Y (2001a) Ionospheric tomography using GPS measurements. In: Proceeding of the international symposium on kinematic systems in geodesy, geomatics and navigation, Banff, 5–8 Jun 2001, pp 111–120
- Liu ZZ, Gao Y (2001b) Optimization of parameterization in ionospheric tomography. In: Proceeding of institute of navigation GPS 2001, Salt Lake City, Utha, 11–14 Sep 2001, pp 2277–2285
- Mashhad Hossainali M (2006) A comprehensive approach to the analysis of the 3D kinematics of deformation. Institute of Physical Geodesy. PhD Thesis, Darmstadt University of Technology, Darmstadt, p 152
- Mitchell CN, Kersley L, Heaton JAT, Pryse SE (1997) Determination of the vertical electron-density profile in ionospheric tomography: experimental results. *Ann Geophys* 15:747–752
- Nohuteu M, Karslioglu MO, Schmidt M (2010) B-spline modeling of VTEC over Turkey using GPS observations. *J Atmos Sol Terr Phys* 72(7–8):617–624. doi:10.1016/j.jastp.2010.02.022
- Raymund TD, Pryse SE, Kersley L, Heaton JAT (1993) Tomographic reconstruction of ionospheric electron density with European incoherent scatter radar verification methods. *Radio Sci* 28:811–818
- Schaer S (1999) Mapping and predicting the earth's ionosphere using the global positioning system. PhD Dissertation, Astronomical Institute, University of Berne, p 205
- Seeber G (1993) Satellite geodesy: foundations, methods and application. Walter de Gruyter, Berlin and New York, p 531
- Skone S (1998) Wide area ionosphere grid modeling in the auroral region. UCGE reports number 20123, PhD Thesis, The University of Calgary, Calgary
- Strangeways HJ, Kutiev I, Cander LR et al (2009) Near-earth space plasma modelling and forecasting. *Ann Geophys* 52(3–4):255–271
- Walker JK (1989) Spherical cap harmonic modeling of high latitude magnetic activity and equivalent sources with sparse observations. *J Atmos Terr Phys* 51(2):67–80
- Yin P, Mitchell CN, Spencer PSJ, Foster JC (2004) Ionospheric electron concentration imaging using GPS over the USA during the storm of July 2000. *Geophys Res Lett* 31:L12806
- Yizengaw E, Moldwin MB, Dyson PL, Essex EA (2007) Using tomography of GPS TEC to routinely determine ionospheric average electron density profiles. *J Atmos Solar Terr Phys* 69:314–321